

## A MINI X-RAY SURVEY OF SUB-DLAs; SEARCHING FOR AGNs FORMED IN PROTOGALAXIES

G. CHARTAS<sup>1,2</sup>, V. P. KULKARNI<sup>2</sup>, AND A. ASPER<sup>1</sup>

*Received 2013 May 16; Accepted 2013 July 21*

### ABSTRACT

A significant fraction of the sub-damped Lyman-alpha (sub-DLA) absorption systems in quasar spectra appear to be metal-rich, many with even super-solar element abundances. This raises the question whether some sub-DLAs may harbor active galactic nuclei (AGN) since supersolar metallicities are observed in AGN. Here we investigate this question based on a mini-survey of 21 quasars known to contain sub-DLAs in their spectra. The X-ray observations were performed with the *Chandra X-ray Observatory*. In cases of no detection we estimated upper limits of the X-ray luminosities of possible AGNs at the redshifts of the sub-DLAs. In six cases we find possible X-ray emission within  $\sim 1''$  of the background quasar consistent with the presence of a nearby X-ray source. If these nearby X-ray sources are at the redshifts of the sub-DLAs, their estimated 0.2–10 keV luminosities range between  $0.8 \times 10^{44} h^{-2}$  and  $4.2 \times 10^{44} h^{-2} \text{ erg s}^{-1}$ , thus ruling out a normal late-type galaxy origin, and suggesting that the emission originates in a galactic nucleus near the center of a protogalaxy. The projected distances of these possible nearby X-ray sources from the background quasars lie in the range of 3–7  $h^{-1}$  kpc, consistent with our hypothesis that they represent AGNs centered on the sub-DLAs. Deeper follow-up X-ray and optical observations are required to confirm the marginal detections of X-rays from these sub-DLA galaxies.

*Subject headings:* galaxies: formation — galaxies: evolution — quasars: absorption lines — X-rays: galaxies — intergalactic medium

### 1. INTRODUCTION

The galaxy formation process is thought to be hierarchical with smaller dark matter haloes coalescing to form larger ones (e.g., for a review see Springel, Frenk & White, 2006, and references therein). According to this theory when the baryonic matter cools down enough to form molecular hydrogen it falls into these haloes resulting in the birth of the first stars. Eventually clusters of stars may form in the centers of these haloes. The merger of these haloes may produce the first protogalaxies.

The damped and sub-damped Lyman-alpha absorption line systems found in quasar and GRB spectra are thought to be produced by intervening protogalaxies or young galaxies (e.g., Wolfe, Gawiser, & Prochaska 2005, and references therein). The damped Lyman-alpha (DLA) absorbers have neutral hydrogen column densities  $\log N_{\text{HI}} \geq 20.3$ , while sub-DLAs have  $19.0 \leq \log N_{\text{HI}} < 20.3$ . Together, DLAs and sub-DLAs constitute most of the neutral hydrogen in galaxies at high redshifts. The nature of the protogalaxies associated with DLAs and sub-DLAs is very uncertain. To understand where DLA/sub-DLAs fit in the big picture of galaxy evolution, it is of great interest to understand the nature of the galaxies associated with DLA/sub-DLA absorbers.

Recent observations of element abundances show most DLAs to be metal-poor, while a substantial fraction of sub-DLAs appear to be metal-rich, i.e., near-solar or even super-solar; (see, e.g., Kulkarni et al. 2005, 2007, 2010; Prochaska et al. 2003, 2006; Peroux et al. 2006; Meiring et al. 2008, 2009). A small fraction (about 5%) of DLAs are also found to be metal-strong (Herbert-Fort

et al. 2006). How did these metal-rich absorbers get so enriched > 7–10 Gyr ago? Supersolar metallicities are also found in AGN at both low and high redshifts, from emission-line observations (e.g., Storchi-Bergmann et al. 1998; Hamann et al. 2002; Dietrich et al. 2003; Nagao et al. 2006; Groves et al. 2006). The presence of AGN with supersolar metallicity at even  $z \sim 5$  may seem surprising given that galaxies at high redshifts are expected to be more gas-rich, and less enriched compared to low-redshift galaxies (e.g., Kauffman & Haehnelt 2000). The first major star formation episode in the high-redshift metal-rich AGN appears to have happened at  $< 1$  Gyr after the Big Bang. In any case, the observations of high metallicities in AGN at high and low redshifts, together with the existence of metal-rich sub-DLA absorbers, raises the question of whether some of the metal-rich *absorbers* may be associated with galaxies possessing AGN powered by super-massive black holes (SMBH).

Indeed, the process by which supermassive black holes form and grow at the centers of galaxies is also very uncertain. Proposed models of SMBH formation and growth (e.g., Kauffmann & Haehnelt 2000; Wyithe & Loeb 2003; Volonteri et al. 2003; Hopkins et al. 2006; Croton et al. 2006; Volonteri et al. 2013) include: (a) the direct collapse from dense cold gas clouds, (b) contraction of dense cold gas into a supermassive star that after fragmentation or multiple formation events may form black hole binaries that spiral together via gravitational radiation to form a SMBH, (c) runaway growth of a massive black hole by accretion, (d) mergers of black holes and (e) more realistically, a combination of the above models.

It is unknown at what exact time during a galaxy's formation period the central massive black hole accretes enough gas to become active. A rough estimate of the duration of the active phase can be obtained from the

<sup>1</sup> Department of Physics and Astronomy, College of Charleston, Charleston, SC, 29424, USA, chartasg@cofc.edu

<sup>2</sup> Department of Physics and Astronomy, University of South Carolina, Columbia, SC, 29208, USA, kulkarni@sc.edu

observed fraction of galaxies that contain active nuclei. Specifically, surveys of galaxies indicate that about one in every hundred contain active nuclei implying AGN lifetimes of the order of  $10^8$  years. It is thought that an AGN's lifetime will depend on the amount of time it takes for the accretion rate to drop below a critical level.

Typical quasars and Seyfert galaxies require accretion rates of the order of a few  $M_{\odot}$  per year to be active, whereas, the accretion rate onto a non-active nucleus such as SgrA\* is  $\sim 10^{-9} - 10^{-8} M_{\odot}$  per year (e.g., Dexter et al. 2009; Shcherbakov et al. 2012). There are various proposed processes that can lead to the reduction of the available gas reservoir that feeds the central source. These include the ejection of gas from the galaxy by powerful AGN and starburst winds, the formation of stars and the infall of gas into the central black hole.

In protogalaxies these processes have not had enough time to deplete the gas reservoir and protogalaxies may contain enough gas to fuel a possible central massive black hole. If this is the case, we might expect to find a large fraction of protogalaxies with active nuclei. The protogalaxies sampled by metal-rich DLAs and sub-DLAs could thus be associated with SMBH with undepleted gas reservoirs. Examples of AGN in local analogues to protogalaxies are the actively accreting massive black hole detected in the dwarf starburst galaxy Henize2-10 (Reines et al. 2011,2012) and AGN detected in local galaxies with properties that are very similar to distant Lyman-break galaxies (Jia et al. 2011).

In §2 we present our sample of sub-DLAs and the analysis of X-ray observations; in §3 we discuss the possible detection of X-rays near the locations of background quasars that are known to contain sub-DLAs; and in §4 we present a discussion of our results and prospects for expanding the sample and improving the confidence of the detections. Throughout this paper we adopt a flat  $\Lambda$  cosmology with  $H_0 = 70 h \text{ km s}^{-1} \text{ Mpc}^{-1}$ ,  $\Omega_{\Lambda} = 0.7$ , and  $\Omega_M = 0.3$ .

## 2. SUB-DLA SAMPLE AND X-RAY OBSERVATIONS

To test the plausibility that sub-DLAs may be associated with SMBHs we performed an exploratory search for X-ray emission associated with a subset of the sub-DLAs presented in a survey of  $z > 4$  quasars (Guimaraes et al. 2009). We also included five sub-DLAs detected in additional studies (Peroux et al., 2011; Prochaska et al. 2005; Som et al. 2013)

These sub-DLAs were chosen because X-ray spectra of their background quasars have been obtained with the *Chandra X-ray Observatory* (hereafter *Chandra*) and are available in the *Chandra X-ray Center* archives. Our search was restricted to *Chandra* observations since only *Chandra* has the spatial resolution of  $\sim 0''.5$ ; high spatial resolution is desirable to resolve X-ray emission from the candidate protogalaxies associated with the sub-DLAs. As a result of this search we found 21 quasars with sub-DLAs that had been observed with the Advanced CCD Imaging Spectrometer (ACIS; Garmire 2003) on board *Chandra*. A log of the X-ray observations that includes observation dates, observational identification numbers, exposure times, ACIS frame time and the observed 0.2–10 keV counts is presented in Table 1.

## 3. X-RAY MINI-SURVEY OF SUB-DLAs

The *Chandra* observations of the sub-DLAs of our mini-sample were analyzed using the standard software CIAO 4.5 provided by the *Chandra X-ray Center* (CXC). We used standard CXC threads to screen the data for status, grade, and time intervals of acceptable aspect solution and background levels. To improve the spatial resolution we employed the sub-pixel resolution technique developed by Li et al. (2004) and incorporated via the Energy-Dependent Subpixel Event Repositioning (EDSER) algorithm into the tool `acis_process_events` of CIAO 4.5. For comparison we also employed the sub-pixel resolution technique developed by Tsunemi et al. (2001). In 17 out of 21 cases the background quasar is detected with *Chandra*. In 6 out of the 21 *Chandra* observations we detected X-ray emission (resolved from the quasar itself) within  $\sim 1''$  of the background quasar that is known to contain a sub-DLA in its optical/UV spectrum. One exciting possibility is that this X-ray emission originates from an AGN near the center of a protogalaxy. In Figure 1 we show the *Chandra* images of the fields around quasars PSS 0121+0347, PSS 0133+0400, PSS 0955+5940, SDSS J095744.46+330820.7, Q 1323–0021, and PSS 2322+1944, near which we detected X-ray emission possibly associated with the intervening systems. The *Chandra-ACIS* Point Spread Function (PSF) has a FWHM of  $\sim 0''.5$ , and is indicated with the solid circles centered on the optical positions of the quasars. We detect X-rays centered on the background quasars, however, we also detect a significant number of counts asymmetrically distributed and located about  $0.5 - 1''$  from the optical positions of the quasars. Regions containing  $\geq 3$  events with a distance of greater than 0.5 arcsec from the background quasar and clustered within a 0.5 arcsec radius circle were considered as marginally detected X-ray sources. The dashed circles are centered on the marginally detected X-ray emission within  $\sim 1''$  of the background quasars. In Table 2 we list the properties of the background quasars and their sub-DLAs.

The spatial distributions of the excess X-ray counts near the quasars are consistent with being produced by point sources in the sense that these counts are clustered within circles of radii of less than  $0''.5$  (ACIS PSF FWHM  $\sim 0''.5$ ). X-ray emission from the host galaxy is too weak to be detected at the redshift of the quasar. PSS 2322+1944 is a gravitationally lensed quasar with the second lensed image represented with a circle near label B in Figure 1. We find a marginal detection of X-ray counts near the location of the second lensed image. We note that the background in these *Chandra* observations is very low as evident with the very few counts detected away from these sources. In Figure 2 we also show the observed surface brightness profiles centered on the quasars Q 1323-0021 and PSS 2322+1944 and compare them to simulated ones for a point source. The other four candidates have too few counts to produce surface brightness profiles. We employed the MARX tool to simulate PSFs. The observed surface brightness profiles deviate from those simulated for a single point source and the presence of additional sources within  $1''$  of the quasar is consistent with our image analysis. We note that these

quasars were centered on-axis at the aim-point of ACIS S3.

In the case of the moderate S/N image of Q 1323-0021, the detected counts were sufficient for a two-dimensional fit to both the background quasar and nearby X-ray sources with simulated PSFs. The image was binned with a bin size of  $0''.0246$  bins (compared to the  $0''.491$  ACIS pixel scale) and fit by minimizing the  $C$ -statistic (Cash 1979) between the observed and model images. In Figure 3 we show the best-fit PSF model of the *Chandra* observation of Q 1323-0021. The positions of the PSFs were left as free parameters in the fit and the best-fit values of the positions of the nearby sources labelled as S1 and S2 are listed in Table 3. S1 and S2 lie at angular separations of  $0''.47$  and  $0''.43$  respectively from the background quasar. Neither S1 nor S2 is seen in the  $K'$ -band adaptive optics image with FWHM  $0''.08$  obtained by Chun et al. (2010). However, we note that a massive candidate galaxy was reported by Chun et al. (2010) to be located  $1''.25$  away from the quasar. It is possible that S1 and S2 are not bright enough in near-IR, or they are lost in the artifacts of the AO PSF in the image of Chun et al. (2010). We note that the intervening absorber of Q 1323-0021 is one of the highest metallicity absorbers known. Specifically, Péroux et al. (2006) reported metallicities of  $[\text{Zn}/\text{H}] = +0.61 \pm 0.20$  and  $[\text{Fe}/\text{H}] = -0.51 \pm 0.20$ .

#### 4. DISCUSSION AND CONCLUSIONS

Our exploratory mini-survey of sub-DLAs contained mostly short snapshot *Chandra* observations with exposure times ranging between 2-19 ks. In 17 of the 21 *Chandra* observations of the sub-DLA fields in our sample we detect X-rays from the background quasars that are known to contain the sub-DLAs. In the *Chandra* observations of six quasars of our sample we also have marginal detections of X-ray sources within  $1''$  of the background quasars. These X-ray sources may be associated with the sub-DLAs. We briefly discuss possible origins of these nearby X-ray sources.

(a) X-ray emission from a nearby X-ray source instead of the sub-DLA.

We estimated the probability of detecting a background X-ray source within a circle of radius  $1''$  centered on the quasar by scaling the cumulative number counts per square degree found in the 4 Ms *Chandra* Deep Field-South survey (Lehmer et al. 2012) by the ratio of the areas. In Table 3 we list the 0.5–8 keV fluxes of the candidate sub-DLA sources and the probability of finding by chance a second source with a flux greater than or equal to the one detected. We conclude that it is unlikely that our six candidate X-ray sources are random background X-ray sources in the sky. We are being conservative in these estimates since the probability of detecting a faint source near a bright quasar is even smaller than our estimated values.

(b) X-ray emission from normal late-type galaxies instead of the sub-DLA.

X-rays from normal galaxies are thought to be produced by supernovae, supernova remnants, stellar outflows of hot gas, the hot interstellar medium, high and low-mass X-ray binaries and young stars (e.g., Fabbiano 2006). An analysis of normal late-type galaxies detected in the *Chandra Deep Field* survey by Lehmer et al (2012) in-

dicates that their 0.5–8 keV luminosities increase on average from  $\sim 3 \times 10^{39} h^{-2} \text{ erg s}^{-1}$  at  $z = 0.1$  to  $\sim 2 \times 10^{42} h^{-2} \text{ erg s}^{-1}$  at  $z = 1.4$  and their mean X-ray luminosity to star formation rate is found to be constant within this redshift span. An analysis of normal galaxies in the Great Origins Deep Survey fields by Ptak et al. (2007) shows that their X-ray evolution can be expressed as  $L^*(z) = (1+z)^p L^*(z=0)$ , where  $p = 1.6$  for early-type and  $p = 2.3$  for late-type galaxies consistent with what is found in the independent survey of Lehmer et al. (2012). Assuming the nearby X-ray sources detected in our mini-survey are located at the redshifts of the sub-DLAs, their estimated X-ray luminosities (see Figure 3) are significantly larger than what would be estimated if they were originating from normal late-type galaxies at those redshifts.

(c) X-ray emission from AGN associated with the sub-DLAs.

One exciting possibility is that the X-ray emission of the nearby sources of our mini-survey originates from AGN located near the center of the protogalaxy. Assuming the X-ray emission of the nearby sources originates at the redshifts of the intervening sub-DLAs we estimate their 0.2–10 keV luminosities to range between  $0.8 \times 10^{44} h^{-2}$  and  $4.2 \times 10^{44} h^{-2} \text{ erg s}^{-1}$  consistent with that of a low-luminosity AGN. For estimating the luminosities we assumed a power-law model with a photon index of  $\Gamma = 1.8$  modified by Galactic absorption. The angular separation of these X-ray sources from the background quasars correspond to projected linear separations at the redshift of the sub-DLA in the range of  $3\text{--}7 h^{-1} \text{ kpc}$ . These separations are consistent with the expected impact-parameters of the background quasars from the center of the sub-DLAs at the redshift of the foreground absorbers. In Table 3 we provide several properties of the candidate X-ray sources, assuming they are at the redshift of the sub-DLAs.

(d) X-ray emission from an additional image produced by gravitational lensing of the background quasar.

The probability of a quasar being gravitationally lensed into multiple images depends primarily on the comoving number density of lenses and the lensing cross section of each lens and is of the order of 0.1% (e.g, Turner et al. 1984; Comerford et al. 2002). The fraction of background quasars in our sample with a detected candidate nearby X-ray source (6/21) is significantly larger than the expected number of gravitationally lensed quasars in our sample. The probability therefore that any of the quasars in our sample is gravitationally lensed (in addition to PSS 2322 that is a known gravitationally lensed quasar) is negligible. We note that gravitationally lensed quasars are often included in surveys of intervening absorption systems because of their advantage of having multiple lines of sight through intervening absorbers. We searched catalogs of known gravitationally lensed systems (e.g., Master Lens database of the Orphan Lenses Project) and found that none of our candidate X-ray sources are listed as lensed quasars other than PSS 2322.

(e) X-ray emission from intense star formation associated with the sub-DLAs or the host galaxies of the background quasars.

Lehmer et al. (2010) determine the relation between star

formation rate (SFR) and 2–10 keV luminosity ( $L_X^{Gal}$ ) for a sample of galaxies composed of normal galaxies, luminous infrared galaxies (LIRGS) and ultraluminous infrared galaxies ULIRGS to be  $\log(L_X^{Gal}) = \alpha + \beta \log(\text{SFR})$ , where  $\alpha = 39.49 \pm 0.21$ ,  $\beta = 0.74 \pm 0.12$ , and SFR is in units of  $M_\odot \text{ yr}^{-1}$ . We find that the observed 2–10 keV luminosities (listed in Table 3) of the possible X-ray sources near the background quasars are several orders of magnitude larger than the inferred  $L_X^{Gal}$  values assuming the nearby X-ray emission originates from intense star formation associated with the sub-DLAs or the host galaxies of the background quasars.

Follow-up observations with longer exposures are required to confirm or refute the discovery of a possible new class of X-ray sources, in particular ones that may be associated with active protogalactic nuclei. Specifically, spectral and variability analyses of deeper X-ray observations of these sources will increase the S/N of these detections and provide insight into their nature. Follow-up deep spectroscopic and imaging optical and UV observations may also provide the redshifts and images of possible galaxies at the locations of the X-ray sources.

We acknowledge financial support from NASA via the Smithsonian Institution grant SAO AR0-11019X. VPK acknowledges partial support from the National Science Foundation grant AST/1108830.

## REFERENCES

- Baldwin, J. A., Hamann, F., Korista, K. T., et al. 2003, *ApJ*, 583, 649
- Chartas, G., Eracleous, M., Dai, X., Agol, E., & Gallagher, S. 2007, *ApJ*, 661, 678
- Chun, M. R., Kulkarni, V. P., Gharanfoli, S., & Takamiya, M. 2010, *AJ*, 139, 296
- Comerford, J. M., Haiman, Z., & Schaye, J. 2002, *ApJ*, 580, 63
- Croton, D. J., Springel, V., White, S. D. M., et al. 2006, *MNRAS*, 365, 11
- Dexter, J., Agol, E., & Fragile, P. C. 2009, *ApJ*, 703, L142
- Dietrich, M., Hamann, F., Shields, J. C., et al. 2003, *ApJ*, 589, 722
- Ellison, S. L., Prochaska, J. X., & Mendel, J. T. 2011, *MNRAS*, 412, 448
- Fabbiano, G. 2006, *ARA&A*, 44, 323
- Garmire, G. P., Bautz, M. W., Ford, P. G., Nousek, J. A., & Ricker, G. R. 2003, *Proc. SPIE*, 4851, 28
- Groves, B. A., Heckman, T. M., & Kauffmann, G. 2006, *MNRAS*, 371, 1559
- Guimarães, R., Petitjean, P., de Carvalho, R. R., et al. 2009, *A&A*, 508, 133
- Hamann, F., Korista, K. T., Ferland, G. J., Warner, C., & Baldwin, J. 2002, *ApJ*, 564, 592
- Herbert-Fort, S., Prochaska, J. X., Dessauges-Zavadsky, M., et al. 2006, *PASP*, 118, 1077
- Hopkins, P. F., Hernquist, L., Cox, T. J., et al. 2006, *ApJS*, 163, 1
- Jia, J., Ptak, A., Heckman, T. M., et al. 2011, *ApJ*, 731, 55
- Kauffmann, G., & Haehnelt, M. 2000, *MNRAS*, 311, 576
- Kulkarni, V. P., Fall, S. M., Lauroesch, J. T., et al. 2005, *ApJ*, 618, 68
- Kulkarni, V. P., Khare, P., Péroux, C., et al. 2007, *ApJ*, 661, 88
- Kulkarni, V. P., Khare, P., Som, D., et al. 2010, *New A*, 15, 735
- Lehmer, B. D., Xue, Y. Q., Brandt, W. N., et al. 2012, *ApJ*, 752, 46
- Li, J., Kastner, J. H., Prigozhin, G. Y., et al. 2004, *ApJ*, 610, 1204
- Meiring, J. D., Kulkarni, V. P., Lauroesch, J. T., et al. 2008, *MNRAS*, 384, 1015
- Meiring, J. D., Lauroesch, J. T., Kulkarni, V. P., et al. 2009, *MNRAS*, 397, 2037
- Nagao, T., Maiolino, R., & Marconi, A. 2006, *A&A*, 447, 863
- Péroux, C., Kulkarni, V. P., Meiring, J., et al. 2006, *A&A*, 450, 53
- Péroux, C., Bouché, N., Kulkarni, V. P., York, D. G., & Vladilo, G. 2011, *MNRAS*, 410, 2237
- Prochaska, J. X., Gawiser, E., Wolfe, A. M., Castro, S., & Djorgovski, S. G. 2003, *ApJ*, 595, L9
- Prochaska, J. X., Herbert-Fort, S., & Wolfe, A. M. 2005, *ApJ*, 635, 123
- Prochaska, J. X., O'Meara, J. M., Herbert-Fort, S., et al. 2006, *ApJ*, 648, L97
- Reines, A. E., & Deller, A. T. 2012, *ApJ*, 750, L24
- Reines, A. E., Sivakoff, G. R., Johnson, K. E., & Brogan, C. L. 2011, *Nature*, 470, 66
- Shcherbakov, R. V., Penna, R. F., & McKinney, J. C. 2012, *ApJ*, 755, 133
- Som, D., Kulkarni, V. P., Meiring, J., York, D. G., Péroux, C., Khare, P., & Lauroesch, J. T. 2013, *MNRAS*, submitted
- Springel, V., Frenk, C. S., & White, S. D. M. 2006, *Nature*, 440, 1137
- Storchi-Bergmann, T., Schmitt, H. R., Calzetti, D., & Kinney, A. L. 1998, *AJ*, 115, 909
- Straka, L. A., Kulkarni, V. P., & York, D. G. 2011, *AJ*, 141, 206
- Tsunemi, H., Mori, K., Miyata, E., Baluta, C., Burrows, D. N., Garmire, G. P., & Chartas, G. 2001, *ApJ*, 554, 496
- Turner, E. L., Ostriker, J. P., & Gott, J. R., III 1984, *ApJ*, 284, 1
- Volonteri, M., Haardt, F., & Madau, P. 2003, *ApJ*, 582, 559
- Volonteri, M., Sikora, M., Lasota, J.-P., & Merloni, A. 2012, *arXiv:1210.1025*
- Wyithe, J. S. B., & Loeb, A. 2003, *ApJ*, 595, 614
- Wolfe, A. M., Gawiser, E., & Prochaska, J. X. 2005, *ARA&A*, 43, 861

TABLE 1  
LOG OF OBSERVATIONS

Object Name	Chandra Observation Date	Chandra Observation ID	RA(2000) <sup>a</sup>	Dec(2000) <sup>a</sup>	$t_{\text{exp}}^b$ (s)	N <sup>c</sup> (counts)	Ref.
PSS 0121+0347	2002 February 07	3151	01 21 26.1	+03 47 07.0	5684	76 ± 9	1
PSS 0133+0400	2001 November 26	3152	01 33 40.3	+04 00 59.0	6076	42 ± 7	1
PSS 0209+0517	2002 January 14	3153	02 09 44.7	+05 17 14.0	5776	28 ± 6	1
SDSS J074749.74+443417.1	2002 December 24	4068	07 47 49.7	+44 34 16.0	4534	9 ± 3	1
SDSS075618+410408	2002 February 08	3032	07 56 18.1	+41 04 08.6	7327	21 ± 5	1
PSS 0955+5940	2002 April 14	3156	09 55 11.3	+59 40 31.0	5681	18 ± 4	1
SDSS J095744.46+330820.7	2001 December 24	3157	09 57 44.4	+33 08 21.0	6035	20 ± 5	1
PSS 1057+4555	2000 June 14	878	10 57 56.3	+45 55 53.0	2807	37 ± 6	1
SDSS J122556.61+003535.1	2006 June 25	6877	12 25 56.6	+00 35 35.1	2885	9 ± 3	2
SDSS J124942.12+334953.8	2001 March 24	2084	12 49 42.2	+33 49 54.0	4619	20 ± 5	1
SDSS J131743.12+353131.8	2000 June 14	879	13 17 43.1	+35 31 31.8	2787	7 ± 3	3
Q1323-0021	2004 May 09	4855	13 23 23.7	-00 21 55.2	4360	151 ± 12	2
SDSS J132512.49+112329.7	2004 March 12	3565	13 25 12.5	+11 23 29.7	4701	32 ± 6	1
SDSS J132611.85+074358.4	2002 January 10	3158	13 26 11.9	+07 43 58.0	5886	72 ± 9	1
	2011 March 07	12794			4982	43 ± 7	1
PSS 1435+3057	2000 May 21	880	14 35 23.0	+30 57 22.0	2881	< 5	1
PSS 1646+5514	2003 September 09	4072	16 46 56.3	+55 14 45.0	4843	7 ± 3	1
SDSS 173744+582829	2002 August 05	3038	17 37 44.9	+58 28 30.0	4616	< 5	1
SDSS J2123-0050	2006 March 30	6822	21 23 29.5	-00 50 53.0	3904	26 ± 5	4
PSS 2322+1944	2002 August 23	3028	23 22 07.1	+19 44 23.0	4897	17 ± 4	1
	2005 August 10	5605			13600	66 ± 8	1
PSS J2344+0342	2003 November 20	4074	23 44 03.2	+03 42 26.0	5099	< 5	1
SDSS J235253.51-002850.4	2002 May 16	2115	23 52 53.5	-00 28 50.4	5779	< 5	2

REFERENCES. — (1) Guimaraes et al. 2009; (2) Peroux et al. 2011; (3) Prochaska et al. 2005; (4) Som et al. 2013

<sup>a</sup>Optical positions in J2000.0 equatorial coordinates.

<sup>b</sup>Effective exposure time after data processing.

<sup>c</sup>Background subtracted source counts for events with energies in the 0.2–10 keV band in a circular region of radius 2''/5 centered on the quasar.

TABLE 2  
 PROPERTIES OF BACKGROUND QUASARS AND SUB-DLAs

Object Name	$z_{\text{em}}$	$z_{\text{abs}}$	$\log N_{\text{G,H}}^a$ $\text{cm}^{-2}$	$\log N_{\text{abs,H I}}^b$ $\text{cm}^{-2}$	$L_{\text{qso}}^c$ $(10^{45} h^{-2} \text{ erg s}^{-1})$	$L_{\text{subDLA}}^d$ $(10^{44} h^{-2} \text{ erg s}^{-1})$
PSS 0121+0347	4.130	2.977	20.544	$19.50 \pm 0.15$	7.1(8.3)	2.1
PSS 0133+0400 <sup>e</sup>	4.154	3.995	20.491	$20.15 \pm 0.10$	3.2(4.2)	2.5
PSS 0209+0517 <sup>e</sup>	4.174	3.862	20.668	$20.30 \pm 0.10$	2.2(2.9)	< 4.0
SDSS J074749.74+443417.1	4.432	3.139	20.719	$20.00 \pm 0.20$	0.84(1.7)	< 4.0
SDSS075618+410408	5.09	4.360	20.685	$20.15 \pm 0.10$	1.9(1.8)	< 3.8
PSS 0955+5940	4.336	3.843	20.134	$20.00 \pm 0.15$	2.1(1.7)	4.2
		4.044		$20.10 \pm 0.15$		4.7
SDSS J095744.46+330820.7	4.227	3.043	20.179	$19.65 \pm 0.15$	2.6(2.4)	3.6
		3.364		$19.70 \pm 0.15$		4.4
		3.900		$19.50 \pm 0.10$		5.8
PSS 1057+4555	4.137	2.909	20.061	$20.05 \pm 0.10$	5.5(6.4)	< 5.1
		3.058		$19.80 \pm 0.15$		< 5.6
		3.164		$19.50 \pm 0.20$		< 6.0
		3.317		$20.15 \pm 0.10$		< 6.6
SDSS J122556.61+003535.1	1.226	0.773	20.283	$21.38 \pm 0.12$	0.18(0.37)	< 0.36
SDSS J124942.12+334953.8	4.897	4.572	20.097	$19.80 \pm 0.10$	4.3(4.2)	< 11
SDSS J131743.12+353131.8	4.381	3.461	19.998	$19.90 \pm 0.05$	1.1(2.1)	< 9.3
Q1323-0021	1.388	0.716	20.270	$20.21 \pm 0.20$	2.2(2.2)	0.5(S1),0.5(S2)
SDSS J132512.49+112329.7	4.400	3.723	20.281	$19.50 \pm 0.20$	4.9(4.1)	< 5.7
		4.133		$19.50 \pm 0.20$		< 6.9
SDSS J132611.85+074358.4 <sup>e</sup>	4.123	2.919	20.303	$19.95 \pm 0.10$	6.7(6.9)	< 2.5
		3.425		$19.90 \pm 0.15$		< 3.5
SDSS J132611.85+074358.4 <sup>f</sup>	4.123	2.919	20.303	$19.95 \pm 0.10$	6.5(5.8)	< 3.9
		3.425		$19.90 \pm 0.15$		< 5.3
PSS 1435+3057	4.350	3.267	20.068	$20.05 \pm 0.10$	< 1.3	< 7.5
		3.516		$20.20 \pm 0.10$		< 8.7
		3.778		$19.85 \pm 0.10$		< 10.0
PSS 1646+5514	4.084	2.932	20.382	$19.50 \pm 0.10$	0.95(0.78)	< 5.1
	4.084	4.029		$19.80 \pm 0.15$		< 9.3
SDSS 173744+582829	4.940	4.152	20.550	$19.85 \pm 0.15$	< 8.1	< 66.0
SDSS J2123-0050	2.261	2.058	20.667	$19.35 \pm 0.10$	1.2(1.4)	< 2.2
PSS 2322+1944 <sup>g</sup>	4.118	2.888	20.655	$19.95 \pm 0.10$	$2.0\mu_X^{-1}(1.8\mu_X^{-1})$	< 3.0
		2.975		$19.80 \pm 0.10$		< 3.2
PSS 2322+1944 <sup>h</sup>	4.118	2.888	20.655	$19.95 \pm 0.10$	$2.7\mu_X^{-1}(2.6\mu_X^{-1})$	1.1(S1),0.89(S2)
		2.975		$19.80 \pm 0.10$		1.2(S1),0.96(S2)
PSS J2344+0342	4.239	3.884	20.735	$19.80 \pm 0.10$	< 0.9	< 0.8
SDSS J235253.51-002850.4	1.628	0.873	20.543	$19.18 \pm 0.10$	< 0.09	< 0.2
		1.032		$19.81 \pm 0.13$		< 0.3
		1.247		$19.60 \pm 0.25$		< 0.5

<sup>a</sup>Total Galactic hydrogen column density from Dickey & Lockman (1990)

<sup>b</sup>H I column density.

<sup>c</sup>0.2–10 keV luminosity of background quasar assuming a spectral model consisting of a power-law with a photon index fixed at  $\Gamma = 1.8$  and Galactic absorption. The values listed in parenthesis represent 0.2–10 keV luminosities obtained from spectral fits assuming the same model where the photon index was allowed to vary.

<sup>d</sup>Upper limit of the 0.2–10 keV luminosity of the sub-DLA assuming a 5 count detection within a circle of radius  $0''.5$ . In cases with detected nearby sources we list the observed 0.2–10 keV luminosities of the subDLA's. In cases where two sources are detected near the background quasar, the luminosity of each source is followed by its label shown in Figure 1.

<sup>e</sup>The estimated luminosities correspond to the 2002 January 10 observation of SDSS J132611.85+074358.4

<sup>f</sup>The estimated luminosities correspond to the 2011 March 7 observation of SDSS J132611.85+074358.4

<sup>g</sup>The estimated luminosities correspond to the 2002 August 20 observation of PSS 2322+1944. We have assumed that the model-predicted magnification in the optical band of  $\mu_{\text{opt}} \approx 4.7$ , (Riechers et al. 2008) is equal to the X-ray magnification,  $\mu_X$ .

<sup>h</sup>The estimated luminosities correspond to the 2005 August 10 observation of PSS 2322+1944.

TABLE 3  
PROPERTIES OF CANDIDATE X-RAY SOURCES

Quasar	$z_{\text{em}}$	$z_{\text{abs}}$	$\log N_{\text{HI}}^a$ ( $\text{cm}^{-2}$ )	$\Delta x^b$ ( $''$ )	$\Delta y^b$ ( $''$ )	$D^c$ (kpc)	$f_{0.2-10}^d$	$L_{2-10}^e$	$P^f$ $10^{-4}$
PSS 0121+0347	4.130	2.977	19.50	+0.28	+0.68	5.71	3.84	1.8	2.4
PSS 0133+0400	4.154	3.995	20.15	+0.72	+0.73	7.16	2.94	2.2	2.9
PSS 0955+5940	4.336	3.843	20.00	+0.58	+0.19	4.31	4.80	3.4	1.9
PSS 2322+1944 (S1)	4.118	2.888	19.95	+0.72	-0.50	6.85	2.58	0.94	3.1
PSS 2322+1944 (S2)				-0.50	+0.38	4.90	2.09	0.75	3.9
Q 1323-0021 (S1)	1.388	0.716	20.21	+0.42	+0.22	3.39	33.3	0.3	0.17
Q 1323-0021 (S2)				-0.17	+0.39	3.10	33.3	0.3	0.17
SDSS J095744.46+330820.7	4.227	3.043	19.65	-0.44	-0.34	4.29	6.4	2.7	1.4

<sup>a</sup>Hydrogen column density of sub-DLA.

<sup>b</sup>The RA and Dec offsets of the centroids of the candidate X-ray sources detected near the quasars. In cases where two nearby sources are detected they are labelled as S1 and S2 (see Figure 1).

<sup>c</sup>The projected distances of these candidate X-ray sources from the quasars (scale lengths calculated at  $z_{\text{abs}}$ ).

<sup>d</sup>The observed 0.2–10 keV fluxes of these candidate X-ray sources in units of  $10^{-15} \text{ erg s}^{-1} \text{ cm}^{-2}$ .

<sup>e</sup>Absorbed 2–10 keV luminosity for a source at  $z_{\text{abs}}$  in units of  $10^{44} h^{-2} \text{ erg s}^{-1}$ . To estimate the luminosity we have assumed a power-law model with a photon index fixed at  $\Gamma = 1.8$  modified by Galactic absorption.

<sup>f</sup>The probability of finding by chance a background X-ray source within a circle of radius  $1''$  centered on the quasar with a flux greater than or equal to the one detected.



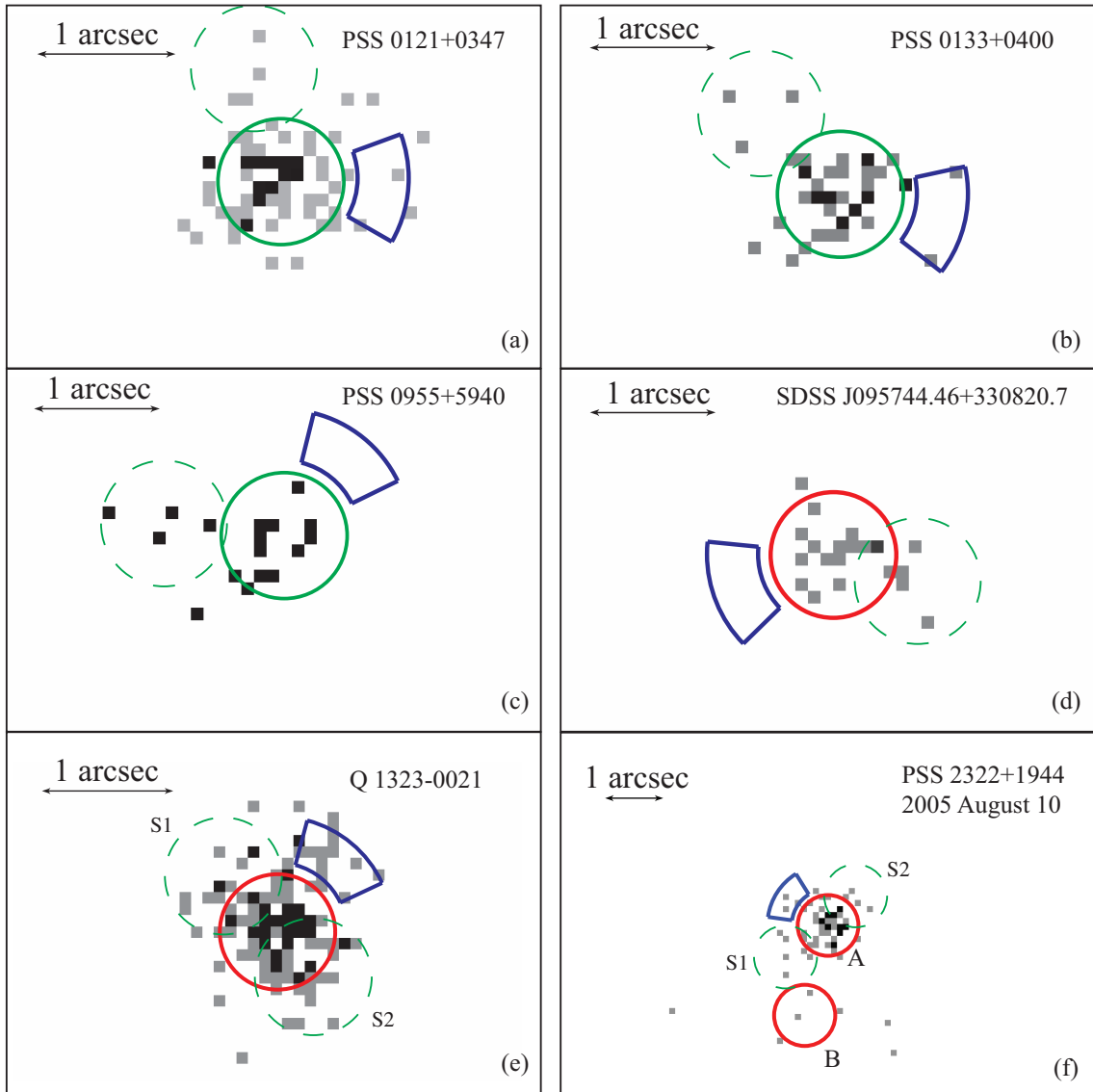


FIG. 1.— *Chandra* images of the fields near quasars PSS 0121+0347 (a), PSS 0133+0400 (b), PSS 0955+5940 (c), SDSS J095744.46+330820.7 (d), Q 1323-0021 (e), and PSS 2322+1944 (f). The solid circles are centered on the background quasars and have radii of  $0''.5$ , which is approximately the size of the point spread function of *Chandra-ACIS* on axis. The images suggest the presence of X-ray sources within  $\sim 1''$  of the quasars. The dashed circles are centered on possible nearby X-ray sources. PSS 2322+1944 is a known gravitationally lensed quasar with images A and B separated by  $\sim 1''.5$ . Background noise in these *Chandra* observations is negligible as evident from the lack of events just a few arcsec away from the central sources. The X-ray sources we report (denoted as dashed circles) are not near the locations of the PSF artifacts (denoted as pie-shaped regions). North is up and east is to the left.

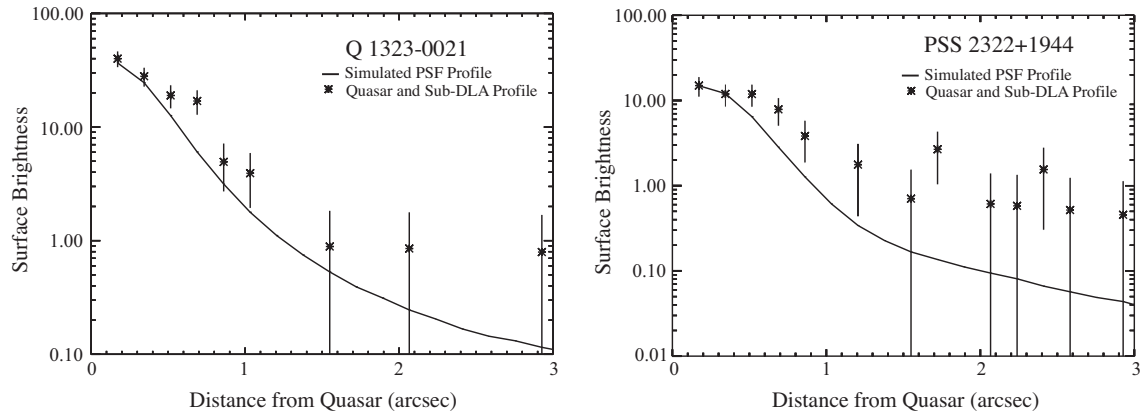


FIG. 2.— Observed surface brightness profiles of the X-ray emission centered on quasars Q 1323–0021 and PSS 2322+1944. For PSS 2322+1944 we stacked the images from the 2002 and 2005 observations. The solid lines represent simulated surface brightness profiles of point sources. The observed X-ray surface brightness profiles deviate significantly from those of point sources at distances of about  $0''.5$  from the quasar, consistent with the presence additional nearby point sources as shown in Figure 1. In the case of PSS 2322+1944 the observed deviations at distances larger than  $0''.5$  are possibly due to lensed image B located about  $1''.5$  from the brighter image A.

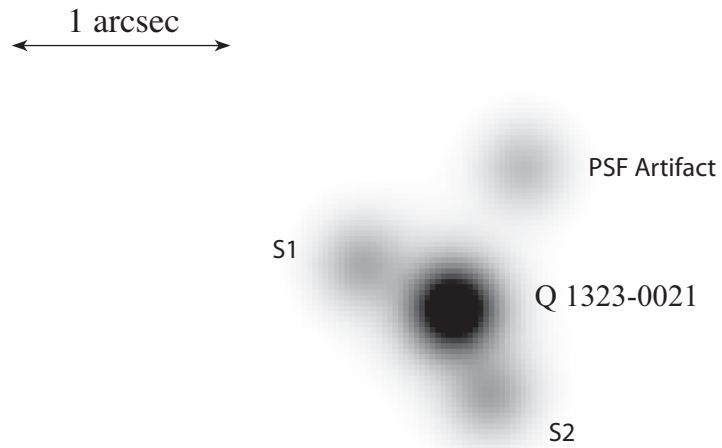


FIG. 3.— Best-fit PSF model to the *Chandra* observation of Q 1323–0021. North is up and east is to the left.

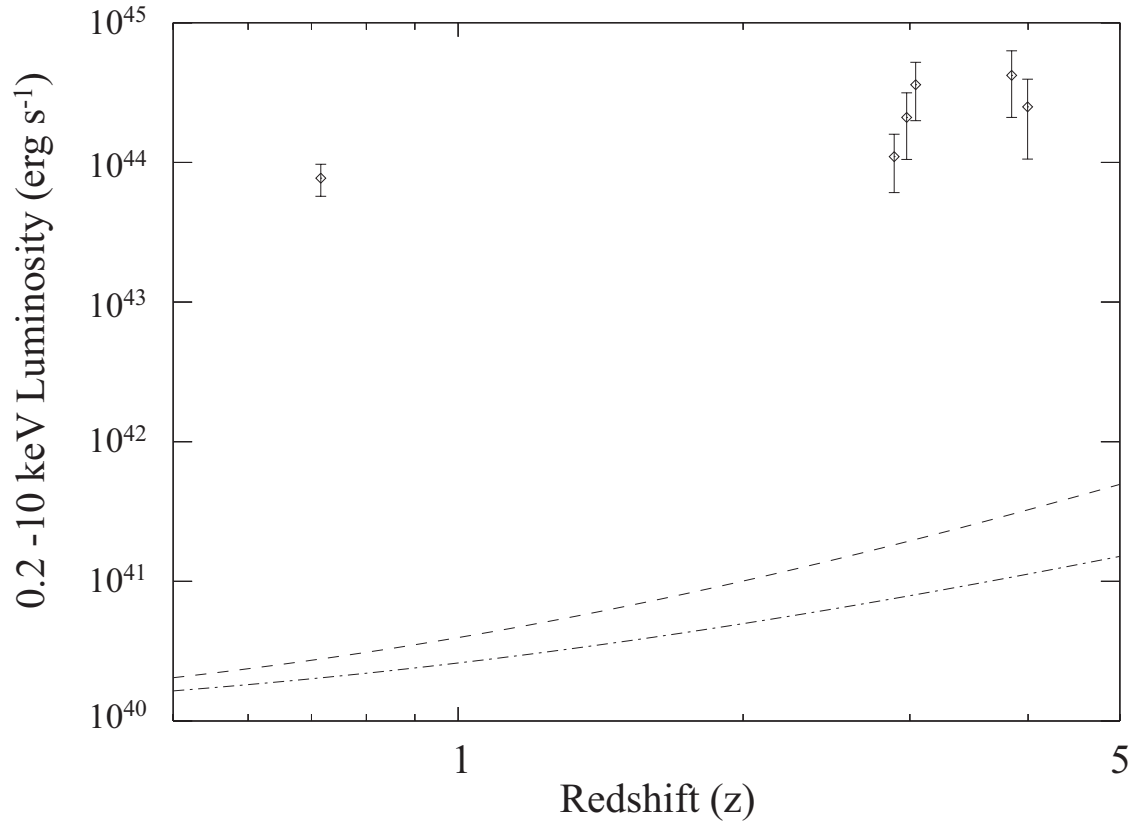


FIG. 4.— 0.2–10 keV luminosities of candidate X-ray sources possibly associated with sub-DLAs versus redshift. The dashed and dot-dashed lines represent the predicted X-ray luminosity evolution of normal late-type and early-type galaxies, respectively, presented in Ptak et al. (2007) and consistent with the survey of Lehmer et al. (2012).